THE EFFECT OF EXPOSURE LENGTH ON VORTEX INDUCED VIBRATION OF FLEXIBLE CYLINDERS

Zhibiao Rao[1]
Department of Mechanical Engineering
Massachusetts Institute of Technology
Cambridge, MA, USA

Prof. J.Kim Vandiver
Department of Mechanical Engineering
Massachusetts Institute of Technology
Cambridge, MA, USA

Dr.Vikas Jhingran
Shell Exploration and Production International,
Houston, Texas, USA

Dr.Octavio Sequeiros
Shell International Exploration and Production Inc,
Rijswijk, The Netherlands

[1] Corresponding Author, Zhibiao Rao, Email: zbrao@mit.edu

ABSTRACT

This paper addresses a practical problem: "What portion of fairing or strake coverage may be lost or damaged, before the operator must take corrective measures?" This paper explores the effect of lost fairings (the exposure length) on Vortex-Induced Vibration (VIV) of flexible cylinders. The source of data is a recent model test, conducted by SHELL Exploration and Production. A 38m long pipe model with varying amounts of fairings was tested. Response as a function of percent exposure length is reported. Unexpected results are also reported: (i) the flexible ribbon fairings used in the experiment did not suppress VIV at speeds above 1 m/s; (ii) Above 1 m/s, a competition was observed between VIV excited in the faired and bare regions of the cylinder, (iii) Unusual traveling wave behavior was documented—waves generated in the bare region periodically changed direction, and exhibited variation in VIV response frequency.

The results of these tests showed that (1) the excitation on the bare and faired regions could be identified by frequency, because the faired region exhibited a much lower Strouhal number; (2) as expected, the response to VIV on the bare region increased with exposure length; (3) the response to VIV on the faired region decreased with exposure length.

INTRODUCTION

The Vortex-Induced Vibration of flexible cylinders may result in significant fatigue damage. Various suppression devices, like helical strakes and fairings on pipes, have been applied to mitigate the effects of VIV. In 2006, Prof J. Kim Vandiver's MIT research team conducted high mode number VIV field experiments to model vibration suppression, including strakes and fairings [1]. It was found in the second Gulf Stream Experiment that helical strakes successfully mitigate VIV but at the expense of increased drag. It was also found that commercially available hard-shell fairings also suppress VIV and have a lower drag coefficient. The effectiveness of the various fairing configurations were extensively studied by Don W.Allen[2]. A practical problem in the use of strakes or fairings is the unknown consequence of loss of coverage in a particular region. This may be the result of breakage or marine growth. The operator needs to know the consequence of lost effectiveness as a function of the length of the effected region. The experiments reported in the paper specifically address that question.

A series of VIV model tests were conducted by SHELL Exploration and Production in March 2011. One of the objectives was to measure response amplitude as a function of the fraction of missing fairing, herein referred to as the exposure length.

A second objective of this research is to improve response prediction programs, such as SHEAR7, which rely upon the technique known as mode superposition. Therefore, a data analysis technique was employed, which assesses the mode participation factors of participating modes, thus making a direct comparison to predictions possible.

H.Lie and K.E.Kaasen [3] were among early researchers applying the mode superposition method to the task of reconstructing high mode number VIV response from only curvature time series data. Their method assumed orthogonal,

Copyright © 2012 by ASME

sinusoidal mode shapes. In order to reconstruct traveling wave response, which was observed in the Second Gulf Stream Experiment [4], H.Mukundan [5] added fictitious cosine mode shapes in the modal analysis. This had the undesirable affect that the reconstructed displacements were found to have a discontinuity at the boundaries. A window function was recommended by S.I.McNeill [6] to smooth the cosine mode shapes near boundaries so as to force the displacements to match the boundary conditions. This reduces but does not eliminate the problem.

The method of mode reconstruction as described in [3] limits the number of modes used in the analysis to be less than or equal to the number of sensors providing response data. The analyst must adopt a means of deciding which modes to use, within the limitation on the total number of modes. This paper proposes a new method to aid the selection of modes to be used in the reconstruction of VIV response. First the response data is displayed in a wave frequency versus wave number plot, obtained by a two dimensional FFT (2D FFT). Based on the information revealed in the plot, the data is band-pass filtered in both wave frequency and wave number space, thus limiting the range of information to be modeled in the modal reconstruction. The VIV response is then reconstructed from the filtered curvature data. The reconstructed results match very well with the measured data.

The main objectives of this paper were to:
(1) Determine the effect of exposure length on pipes with partial fairing protection.
(2) Analyze the excitation competition between bare and faired regions.
(3) Identify standing & traveling waves.
(4) Evaluate the effectiveness of ribbon fairings.
(5) Improve response reconstruction techniques.

EXPERIMENT DESCRIPTION

The experiments were performed in the MARINTEK Offshore Basin in Trondheim, Norway[7]. The model pipe was a fiberglass tube. The total pipe length was 38 meters and had an outer diameter of 12 mm. The dry mass per unit length was 0.197 kg/m. Additional material properties of the pipe are given in the Table 1.

The exposure length (L_{in}) without fairing was always in the middle of the pipe with the fairings installed symmetrically towards both ends of the pipe, as shown in Figure 1. The exposure length was 0%, 5%, 10%, 15%, 25% or 100%. A picture of the pipe with fairings is shown in Figure 2. The pipe was densely instrumented with 52 equally spaced strain gauges in both cross flow (CF) and in line (IL) directions. The lowest sensor began at 0.717 m from the left end of the pipe in Figure 1. Subsequent sensors were spaced with gaps of 0.717 m. In addition, two tri-axial force transducers were installed at both ends. All transducers were sampled at a rate of 1200 Hz.

The pipe was exposed to both uniform and triangular sheared flow. The maximum flow speed was up to 3.5m/s corresponding to a Reynolds number of ~ 37 000. The data presented in this paper was drawn from 49 separate runs in uniform flow. Only cross-flow response is presented. The pipe tension was approximately constant for each test in the steady state but varied with speed and exposure length from test to test. Mean tensions ranged from 500N to 2500N. The dominant excited mode varied from 4 to 36.

Tab.1: Pipe Model Properties

Length	38.00m	Material	fiberglass
Hydrodynamic diameter	12mm	Strength diameter	10mm
Bending stiffness	16.1 Nm^2	Axial stiffness	780 N
Weight in air	0.197 kg/m	Weight in water	0.078 kg/m
Young modulus	3.27E10 N/ m^2	Mass ratio	1.74

DATA REDUCTION AND ANALYSIS TECHNIQUES

1) 2D-FFT

The 2D FFT technique is a good tool to evaluate the dispersion relation, which is the relation between wave frequency and wave number. For a tension-dominated cable the dispersion relation is:

$$\omega = kc, \quad c = \sqrt{\frac{T}{m+m_a}} \tag{1}$$

Where ω is the wave frequency in radians/second and k is the wave number, c is the phase velocity, T is the tension, m is the mass per unit length, m_a is the added mass per unit length.

The 1D FFT of time series function $f(t)$ is defined as:

$$F(\omega) = \int_{-\infty}^{\infty} f(t)e^{-j\omega t}dt \ , \ f(t) = \frac{1}{2\pi}\int_{-\infty}^{\infty} F(\omega)e^{j\omega t}dt \tag{2}$$

$$\text{Suppose } f(t) = e^{j\omega_0 t}, \ F(\omega) = 2\pi\delta(\omega - \omega_0) \tag{3}$$

Where δ: is the delta function.

Suppose $f(z,t)$ is a function of time and space, then its 2D FFT may be written as :

$$F(\omega,k) = \int_{-\infty}^{\infty}\int_{-\infty}^{\infty} f(z,t)e^{-j(kz+\omega t)}dtdz \tag{4}$$

The Shell tests used 52 strain gauges in the cross-flow direction on the 12 mm diameter pipe to measure vibration. To improve the identification of mode participation factors and to improve the spatial resolution, the two pinned boundary conditions were considered as two additional sensors at which

2 Copyright © 2012 by ASME

the displacement and curvature are zero. Since the 2D FFT uses a series of periodic functions (sine and cosine functions) to best fit the finite-length data set in space, strong edge effects appear near boundaries of pipe. To avoid the strong edge effect, the measured data were assumed to extend symmetrically over a total analysis length equal to three times the cylinder length as shown in Figure 3.

Figure 4 shows the dispersion relation only in the first quadrant for Test2322. Quadrants are defined by the sign of the wave frequency and wave number. If both are positive, it is the first quadrant. Both negative, it is the third quadrant. If wave frequency is positive and wave number is negative, it is the second quadrant. If wave frequency is negative and wave number is positive, it is the fourth quadrant.

Test2322 was a 5% exposure length at a uniform flow speed of 0.5m/s. In Fig.4, the color represents the curvature Fourier coefficients, expressed in dB. Red is the strongest and the blue the weakest. It can be seen that the dominant modes are between 15 and 20. Figure 6 the results of all 5% exposure case in a 3D volumetric plot. One slice portrays the 2D FFT at a particular flow speed. In all tests the exposure length was positioned symmetrically about the middle of the pipe. The slices from lowest to highest flow speed correspond to the experiments numbered Test2322, Test2321, Test2318, Test2319 and Test2320, respectively. The corresponding time series from each test were taken at the following times, measured from the beginning of the test record: 66-71s ,48-53s, 33-38s, 28-33s and 24-29s, respectively. It may be easily seen that at 1 m/s and above the response has two significant frequency components. This higher frequency component is not an integer multiple of the first.

2) $F − K$ Filtering

Filtering Technique. The frequency-wavenumber(f-k) diagram is widely used in the atmospheric sciences and geosciences to visualize atmospheric waves or examine the direction and apparent velocity of seismic waves. Real data have noise of various kinds and are limited in bandwidth due to aliasing in time or space. In these experiments the sampling frequency was very high(1200Hz) and therefore aliasing in the frequency domain was not an issue. However, 52 equally spaced sensors limited the wavenumber bandwidth for reasons of potential spatial aliasing. A frequency-wavenumber, two-dimensional filter was used to remove the noise and prevent spatial aliasing. The basic idea of an *F-K* Filter is to keep the desired information in the frequency-wavenumber diagram and set other unwanted components to zero. A time series of the filtered data may be obtained by a 2D inverse FFT (2D IFFT).

Figure 5 shows the filtered dispersion relation in all quadrants for the same test case test 2322. The filter bandpass values are 5-10 Hz in frequency (f) and 10-45 for mode number corresponding to a wave number of k=0.83-3.72 m^{-1}.

Fourier coefficients in the selected range of frequency (-10, -5) and (5, 10) and the range of mode number (-45,-10) and (10, 45) were kept, while outside of the specified range, the Fourier coefficients were set to zero. The square in Figure 4 demonstrates this by enclosing the desired frequencies and modes/wavenumbers in the first quadrant only.

Two close frequencies are clearly seen in both Figures 4 and Figure 5; the primary response frequency was 7.5Hz with the secondary response frequency at 8.0Hz. This was initially unexpected. Deducing the cause was one of the interesting outcomes of this investigation.

Bare and Faired Regions Excited at Different Frequencies. It is very well known that VIV excitation frequencies are predictable from a Strouhal (*St*) relationship $f_{st} = StU/D$. It was initially expected that the ribbon fairing would entirely suppress VIV. After analyzing the vibration of the fully faired pipe, it was a surprise to find that at flow speeds above 1 m/s that VIV was present in spite of 100% fairing coverage. At high speeds the fairings were not entirely effective. An early hypothesis was that the two frequency components were the result of different Strouhal numbers on the faired and bare regions. To test this required establishing the Strouhal number for fully faired and fully bare pipe. This is shown in Figure 7. The Strouhal numbers corresponding to the faired and bare pipe were found to be 0.088 and 0.143, respectively.

The Strouhal number of the bare pipe is about 1.6 times that of the faired pipe. For experiments with partial coverage and with flow velocities above the threshold velocity of about 1 m/s, two frequencies might be observed with a ratio of 1.6. This brings into the analysis an issue that has been known in the VIV intellectual community but not yet resolved. If a cylinder moves at a frequency different from the locally preferred Strouhal frequency, under what conditions will the presence of this 'foreign' frequency disrupt the local wake synchronization process? In other words, there is the potential in a cylinder with partial fairing coverage to exhibit a competition between two sources of VIV at different frequencies.

It was earlier observed in the 0.5 m/s low speed example shown in Figures 4 and 5, that they were two closely spaced frequency components, at 7.5 and 8.0 Hz. These are not in the ratio of 1.6 to 1.0 and cannot be explained as response from the bare and faired regions. Something else is at work here, which is only revealed after examining the traveling wave properties of the observed response.

Identifying Standing & Traveling Waves. Figure 8 shows the contour plot of filtered curvature, which is obtained by working with the results of the 2D IFFT. The plot shows the amplitude of measured curvature (analogous to strain), expressed in color, as a function of time (horizontal axis). The vertical axis is axial position along the entire length of the cylinder. The

3

Copyright © 2012 by ASME

response is dominated by traveling waves, as indicated by the non-vertical slope of contours of constant color. It may be seen that there are two traveling waves emanating from the exposed region. One is traveling upward and the other is traveling downward. That is to be expected, when the exposed, bare region is in the middle of the pipe as was done in this model test. The exposed region is a power-in region which absorbs VIV energy from the flow, and the faired region becomes the power-out region which dissipates the energy. Waves emanating from the power-in region travel into the faired region, where they attenuate due to damping.

The following analysis procedure was used to study the traveling wave characteristics of the response.

A pure standing wave $f(z,t) = sin(k_0 z)sin(\omega_0 t)$, will have a 2D FFT given by

$$F(\omega, k) = \pi^2 [\delta(k - k_0)\delta(\omega + \omega_0) + \delta(k + k_0)\delta(\omega - \omega_0) - \delta(k - k_0)\delta(\omega - \omega_0) - \delta(k + k_0)\delta(\omega + \omega_0)] \quad (5)$$

A pure traveling wave in the positive z direction, $f(z,t) = sin(k_0 z - \omega_0 t)$, has a 2D FFT given by:

$$F(\omega, k) = 2\pi^2 j[\delta(k + k_0)\delta(\omega - \omega_0) - \delta(k - k_0)\delta(\omega + \omega_0)] \quad (6)$$

For a standing wave, the peaks in a plot of $F(\omega, k)$ will exist in all four quadrants (see Figure 5), while for a pure traveling wave, the peaks of $F(\omega, k)$ will exist in either the first and third or the second and fourth quadrants, depending on the direction of travel.

When the frequency-wave number components of the first and third quadrants (circled in Figure 5) are kept and others are set to zero, the waves traveling downward in Figure 8 are obtained. When the components of the second and fourth quadrants (squared in the Figure 5) are kept and other components are set to zero, the waves traveling in opposite, upward, direction are obtained.

Figure 9 shows the contour plot of the upward traveling wave. It only exists in the upper half part of the pipe. Figure 10 shows the contour plot of the downward traveling wave. It only exists in the lower half part of the pipe. That there are waves traveling both up and down is no surprise, due to the symmetry of the exposed region in the center of the otherwise faired pipe. Closer analysis of the individual traveling wave components revealed an unexpected surprise.

The upward and downward travelling waves alternate in strength with time. The period of time that the upward travelling wave, for example is strong is only about one second. This is not a sufficient record length for conventional FFT analysis to be able to resolve frequencies more closely spaced than 1.0 Hz.

A high resolution technique known as the Maximum Entropy Method (MEM) of spectral analysis was used to resolve the dominant frequency component of the upward and downward traveling wave components[8]. Figure 11 shows the time history of strain gauge number 25 which is located slightly below the coordinate z/L=0.5 as shown in Figures 8, 9 and 10. Figure 12 and Figure 13 show the spectrum of curvature as computed from short time records using MEM. The time window in Figure 12 is from 66.5-68.1s and in Figure 13 from 68.1-69.7s. The peak frequency is 7.5Hz in Figure 12 and 8.0Hz in Figure 13.

Hence, the waves traveling up in the figure are at a slightly different frequency (7.5 Hz) from those travelling down (8.0 Hz). For this experiment, the dominant mode is 17 (Fig.14) and its response frequency is at 7.5Hz. The measured frequency of the downwards traveling wave at 8.0 Hz is very close to the predicted frequency of the 18th mode. Therefore mode switching is observed. This frequency switching between upward and downward traveling waves was commonly observed for the low speed cases, and occasionally observed at high flow speeds. The explanation for this behavior is still unknown and a subject of ongoing research.

3) Modal Reconstruction Analysis

VIV response is generally measured with strain gauges, accelerometers, and occasionally rate sensors, but rarely is displacement measured directly. However, displacement expressed as A/D is most often the desired response quantity, and is felt to be the metric most closely associated with wake synchronization. In this paper the response expressed in terms of A/D is obtained through modal analysis, in which curvature mode shapes are used to identify mode weight, and then the result is converted to an equivalent displacement-based mode participation factor from the known relationship between displacement mode shape and curvature mode shape. The mode superposition method is widely applied to both the prediction of VIV response and to the reconstruction of time domain response at all points on a cylinder from response measured at a limited number of sensors. The mode superposition method can be found in references [3, 5, 6];

Reconstruction Results. Figure 14 and Figure 15 respectively show RMS mode weights of displacement and curvature. There are two different trend lines in the even and odd mode numbers. The dominant odd numbered mode is 17 and the dominant even numbered mode is 18. The mode weight at mode 17 is much larger than that at mode 18. The reason why the mode weights for the odd modes are larger than the even modes is that odd mode shapes are symmetric about the middle of the cylinder, whereas the even modes are anti-symmetric about the center. Since the bare, power-in region is symmetrically located at the center of the cylinder, it favors excitation of modes with symmetric mode shapes. This was born out in the

4   Copyright © 2012 by ASME

mode weights obtained by analysis of the response data as shown in Figures 14 and 15.

Figure 16 shows the comparison of the measured RMS curvature response at available strain gauge locations(blue dots) and reconstructed curvatures (red line) are along the riser. This was done with the data from the same low speed case(Test2322) using the sinusoidal mode shapes corresponding to modes $n = 10$ to $n = 45$. The reconstructed results match well with the measured curvatures. Figure 17 shows the reconstructed displacement for the same test case. The maximum RMS amplitude happens in the power-in region. When waves travel toward the faired region, the VIV amplitudes attenuate due to the hydrodynamic damping caused by fairings. The spatial maximum RMS displacement(A/D) is, however, very small (near 0.02) due to the small power-in region (5% exposure length) and low flow speed (0.5m/s). Figure 18 shows the contour plot of reconstructed curvature, which matches with the original measured curvature quite well (Fig.8). The reconstructed results show that the modal analysis and 2D-FFT filtering techniques, used in this analysis, do a good job capturing important features of the response. It shows that sinusoidal mode shapes are all that is required to accurately model the response. Fictitious cosine mode shapes are not necessary to capture the traveling wave effects.

Excitation Competition on Bare and Faired Regions. At speeds above 1.0 m/s it was previously found that two VIV frequencies are likely to be present in the response, resulting from the bare and faired regions. The F-K analysis method may be used to identify and quantify the two components. Modal analysis may be used to reconstruct the response at all points on the cylinder and may be used to identify which frequency component originates from the bared or faired region

Figure 19 and Figure 20 respectively show reconstructed VIV displacement and curvature of the pipe with larger exposure length (10%) at a larger flow speed (1.5m/s), which corresponds to Test2327. The time window 85-93s was used in the analysis. Before reconstructing the VIV displacement, the curvature data was filtered in both wave frequency and wave number space, thus limiting the range of frequency and wave number information to that known to be most relevant to VIV. The filtering parameters for bare excitation, faired and total excitations are 15-25Hz, 8-15Hz and 8-25Hz for frequency and 20-45, 10-30 and 10-45 for mode number, respectively. The black and blue lines respectively stand for RMS values of VIV response due to only bare excitation and only faired excitation. For bare excitation, exposed region is considered as power-in region and faired region is considered as power-out region. The largest response at the bare excitation frequency happens in the bare region. For faired excitation, exposed region is considered as power-out region and faired region is considered as power-in region. Thus largest response happens in the faired region. Because the length of the bare(exposed) region varies from 5 to 25% of the length, the faired region tends to have greater excitation and therefore greater response. The

red line represents total RMS VIV response due to the both bare and faired excitations. It is not known what effect the response at the faired excitation frequency had on the hydrodynamics of the wake in the bare region.

RESULTS

In order to compare the results from test to test, the same number of vortex shedding cycles rather than the same length of time is used. Due to the size and shape of the ocean basin, the towing distance is approximately the same for each test. Independent of speed the number of vortex shedding cycles is generally constant over the total towing distance for any specific pipe diameter. In the analysis of response data shown here approximately 100 cycles of response data are used for comparing results.

1) Effectivenss of Fairings in Suppressing VIV

Three parameters were defined to analyze the variations of VIV amplitude. They are spatial maximum RMS value, spatial averaged RMS value and the standard deviation at the location of interest.

Spatial Maximum RMS Value: The spatial maximum value is defined as:

$$y_{rms}(z) = \sqrt{\frac{1}{N_T}\left[y^2(z,t_1) + y^2(z,t_2) + \cdots + y^2(z,t_{N_T})\right]} \quad (7)$$

$$y_{max} = max(y_{rms}(z)) \quad (8)$$

Spatial Averaged RMS Value: The spatial average RMS value accounts for the response at all locations:

$$y_{ave} = \frac{y_{rms}(z_1) + y_{rms}(z_2) + \cdots + y_{rms}(z_{N_S})}{N_S} \quad (9)$$

Standard Deviation: Standard deviation is widely used to measure the variance of spatial RMS displacement. A low standard deviation indicates that the spatial RMS displacements tend to be very close to the spatial averaged RMS value, whereas high standard deviation indicates that spatial RMS displacement deviates from the spatial averaged RMS value.

$$\sigma = \sqrt{\frac{1}{N-1}\sum_{i=1}^{N}[y_{rms}(z_i) - y_{ave}]^2} \quad (10)$$

Parameters for Fairing Performance: One objective of this paper is to report on the effectiveness of the fairing used in the experiment. In order to study the performance of fairing, four parameters are defined as percent efficiencies.

$$\eta_1 = \left|\frac{y_{ave}(bare) - y_{ave}(faired)}{y_{ave}(bare)}\right| \times 100 \quad (11)$$

$$\eta_2 = \left|\frac{y_{max}(bare) - y_{max}(faired)}{y_{max}(bare)}\right| \times 100 \quad (12)$$

5

$$\eta_3 = \left| \frac{y_{ave}(bare\ excitation)}{y_{ave}(total\ excitation)} \right| \times 100 \qquad (13)$$

$$\eta_4 = \left| \frac{y_{max}(bare\ excitation)}{y_{max}(total\ excitation)} \right| \times 100 \qquad (14)$$

There are only five runs for the fully faired pipe, there are Test2302, Test2303, Test2304, Test2305 and Test2306 corresponding to flow speeds 0.5m/s, 1.20m/s, 1.32m/s, 1.44m/s and 1.56m/s, respectively. In order to compare VIV response of fully faired pipe with that of bare pipe, some approximations are made due to small number of velocities for the fully faired pipe.

Approximation 1: When there is no flow speed for the fully bared pipe corresponding to the flow speed of fully faired pipe, a linear interpolation was made to find the amplitude at that flow speed of fully faired pipe, expressions (11) and (12) are used to study the efficiency of ribbon fairing.

Approximation 2: For the pipe covered with partial fairings, the bare and faired excitations were separated according to frequency content. Expressions (13) and (14) are used to study the effectiveness of fairing in the suppression of VIV.

The efficiency of the fairing as a function of speed is shown in Figure 21. The black squares were found using expressions (11) or (13). The red dots were estimated using expressions (12) or (14). Figure 21 shows that the efficiency of fairing completely suppressed the VIV at flow speeds below 1m/s. When the flow speed is above 1m/s, the efficiency of fairing decreases to 20-30%.

2) Effect of Explosure Length on VIV

Figure 22 shows the effect of exposure length on VIV amplitude. Markers represent flow speeds varying from 0.5m/s to 2.5m/s. The bar represents the standard deviation of spatial RMS values of displacement.

Bare Excitation: Figure 22 (a) and (b) show respectively the spatial maximum and averaged RMS values of displacement due to bare excitation associated with higher Strouhal number. Both RMS values increase with exposure length, regardless of flow speed. When the bare excitation was separated from the total response, the pipe could be modeled as the power-in region (same as the exposed region) is in the middle of pipe. It was expected that with the increase of the power-in length, more energy enters into the system, which leads to the increase of VIV amplitude.

Faired Excitation: Figure 22 (c) and (d) show respectively the spatial maximum and averaged RMS values of displacement due to faired excitation associated with lower Strouhal number. The test of the pipe with wrapping ribbon fairings was added at the last minute as an extra test of opportunity. There was not time or funding to make up or order airfoil shaped fairings.

These ribbon fairing are inexpensive and readily available, but had unknown performance in suppressing VIV. From Figure 22 (c) and (d), the fairings wholly suppressed the VIV response for lower flow speeds (0.5m/s and 0.75m/s). For higher flow speeds, however, the fairing allowed VIV excitation. More generally, RMS values decreased with increased length of the bare region (decrease of the faired region). When the excitation in the faired region was separated from the total response, the exposed region could be considered as power-out region and the faired region could be modeled as power-in region. It was expected that with the increase of the exposure length, the power-out region increased and the power-in region decreased, thus accompanied by less energy entering into the system, which leads to the decrease of VIV amplitude.

CONCLUSIONS

The primary contribution of this work is that it systematically studies the effect of exposure length on VIV of flexible cylinders with a bare section in the middle.

Summary observations and preliminary conclusions from the VIV analysis of the flexible cylinder with symmetric fairings installed at both sides of the pipe include:
1. The VIV response is dominating by traveling waves for partially faired pipe.
2. Waves periodically changing direction was commonly observed for low speed cases, and occasionally observed at high flow speeds.
3. The flexible ribbon fairings were effective at suppressing VIV at speeds below 1 m/s. Above 1m/s, the fairing still could suppress to 10-30% of typical VIV amplitudes.
4. The excitation on the bare and faired regions could be identified by frequency, because the faired region exhibited a much lower Strouhal number.
5. The response due to excitation on the bare region increases with exposure length.

ACKNOWLEDGMENTS

NOMENCLATURE

1D FFT	One dimensional Fast Fourier Transform
2D FFT	Two dimensional Fast Fourier Transform
c	The phase velocity
D	Hydrodynamic diameter

$f(t)$	Time function
$f(z,t)$	Time and space function
f_{st}	Vortex shedding frequency
$F(\omega)$	The 1D FFT of $f(t)$
$F(\omega, k)$	The 2D FFT of $f(z, t)$
$F - K$	Frequency-Wavenumber
$IFFT$	Inverse Fast Fourier Transform
k	Wave number
L_{in}	Exposure length
m	Mass per unit length
m_a	Added mass
n	Mode number or sine term
N_S	Number of sample in space
N_T	Number of sample in time
RMS	Root mean square
St	Strouhal number
T	Tension
U	Flow speed
ω	Wave frequency in rad/s
$y(z,t)$	VIV time series displacement
y_{ave}	Spatial averaged RMS value of $y_{rms}(z)$
$y_{ave}(bare)$	Spatial averaged RMS displacements for fully bared pipe
$y_{ave}(bare\ excitation)$	Spatial averaged RMS displacement due to bare excitation
$y_{ave}(faired)$	Spatial averaged RMS displacements for fully faired pipe
$y_{ave}(total\ excitation)$	Spatial averaged RMS displacements due to total excitation
y_{max}	Spatial maximum RMS value of $y_{rms}(z)$
$y_{max}(bare)$	Spatial maximum RMS displacements for fully bared pipe
$y_{max}(bare\ excitation)$	Spatial maximum RMS displacements due to bare excitation
$y_{max}(faired)$	Spatial maximum RMS displacements for fully faired pipe
$y_{max}(total\ excitation)$	Spatial averaged RMS displacements due to total excitation
$y_{rms}(z)$	Root mean square of $y(z, t)$
δ	Delta function
σ	Standard deviation of $y_{rms}(z)$
η_1	Parameter 1 of fairing performance
η_2	Parameter 2 of fairing performance
η_3	Parameter 3 of fairing performance
η_4	Parameter 4 of fairing performance

References

[1] Vikas Gopal Jhingran(2008). Drag Amplification and Fatigue Damage in Vortex-Induced Vibrations [D]. Ocean Engineering, Massachusetts Institute of Technology, Boston, USA.

[2] Don W.Allen and Dean L. Henning(2008). Comparisons of Various Fairing Geometries for Vortex Suppression at High Reynolds Numbers. Offshore Technology Conference, OTC 19377.

[3] H.Lie, K.E.Kaasen(2006). Modal analysis of measurements from a large-scale VIV model test of a riser in linearly sheared flow [J]. Journal of fluids and structures, 22(4), P:557-575.

[4] Vivek Jaiswal(2009). Effect of Traveling Waves on Vortex-Induced Vibration of Long Flexible Cylinders[D]. Ocean Engineering, Massachusetts Institute of Technology, Boston, USA.

[5] Harish Mukundan (2008). Vortex-Induced Vibration of Marine Risers: Motion and Force reconstruction from field and experimental data [D]. Ocean Engineering, Massachusetts Institute of Technology, Boston, USA.

[6] S.I.McNeill and P.Agarwal (2011). Efficient Modal Decomposition and Reconstruction of Riser Response due to VIV. OMAE2011-49469.

[7] MARINTEK(2011). Shell Riser VIV Tests Main Report. Main report No.580233.00.01. Norwegian Marine Technology Research Institute.

[8] R.B.Campbell and J. K. Vandiver (1980). "The Determination of Modal Damping Ratios from Maximum Entropy Spectral Estimates", with R. B. Campbell, Proceedings of the 1980 Offshore Technology Conference, Houston, May 1980; also ASME Journal of Dynamic Systems and Control, Vol. 104, March 1982.

Copyright © 2012 by ASME

APPENDIX

Fig.1: Configuration of the pipe with fairings. The exposed region (Bare region) was always in the middle of the pipe and the fairings were installed symmetrically towards both ends of the pipe.

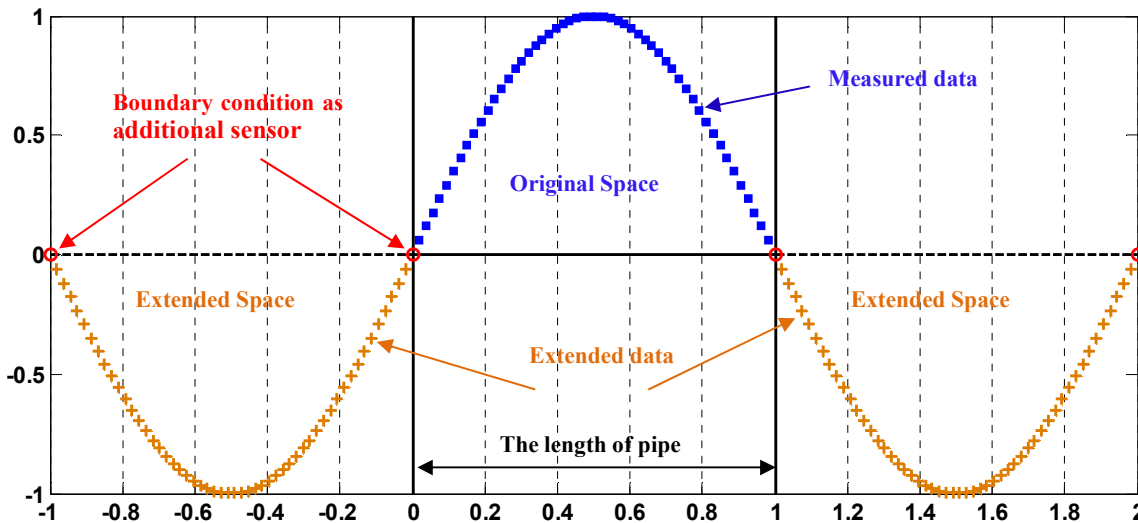**Figure 2: Small pipe covered with wrapping ribbon fairings**

Figure 3 The spatial extension of measured data. The red circles are the ends of the pipe; here they are also considered as four additional sensors with zero displacement in order to increase the resolution in space. The solid blue squares are measured data for 52 strain gauges. The sinusoidal response at one specific time is assumed. The orange crosses represent the extended data. In the left extended space, the extended data are symmetric about point (0, 0) with the measured data for any point in time. In the right extended space, the extended data are symmetric about point (1, 0) with the measured data for any point in time.

8

Copyright © 2012 by ASME
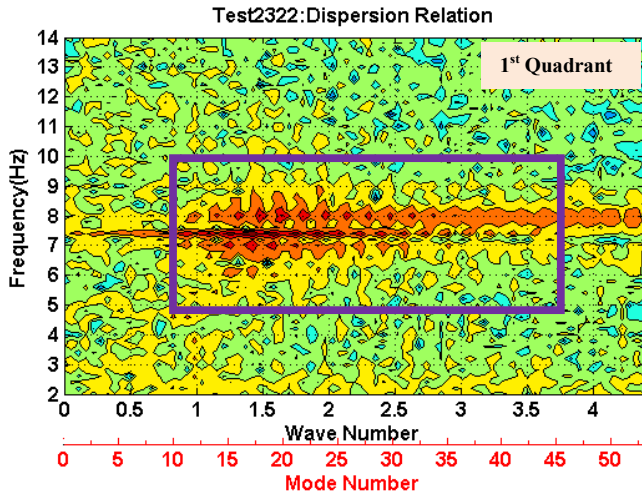
Figure 4: Dispersion relation plot only in the first quadrant with 2D FFT to all curvatures for Test 2322. Test 2322 corresponds to 5% exposure length in the middle of the pipe under uniform flow 0.5m/s. The time section 66s to 71s was used. The color repents the Fourier coefficients of curvatures in dB. Red is the strongest and blue the weakest.
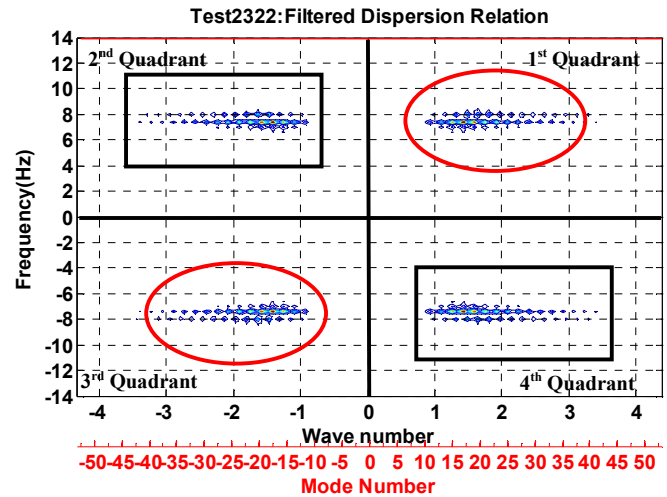
Figure 5: Filtered dispersion relation plot in all quadrants with 2D FFT to all curvatures for Test 2322. The filtered parameters are 5-10Hz for wave frequency (f) and 10-45 for mode number corresponding to 0.83-3.72 for wave number(k). 2D IFFT of circled peaks in the first and third quadrants are waves traveling from right to left or from top to bottom, while 2D IFFT of squared peaks in the second and fourth quadrants are waves traveling from left to right or from bottom to top.
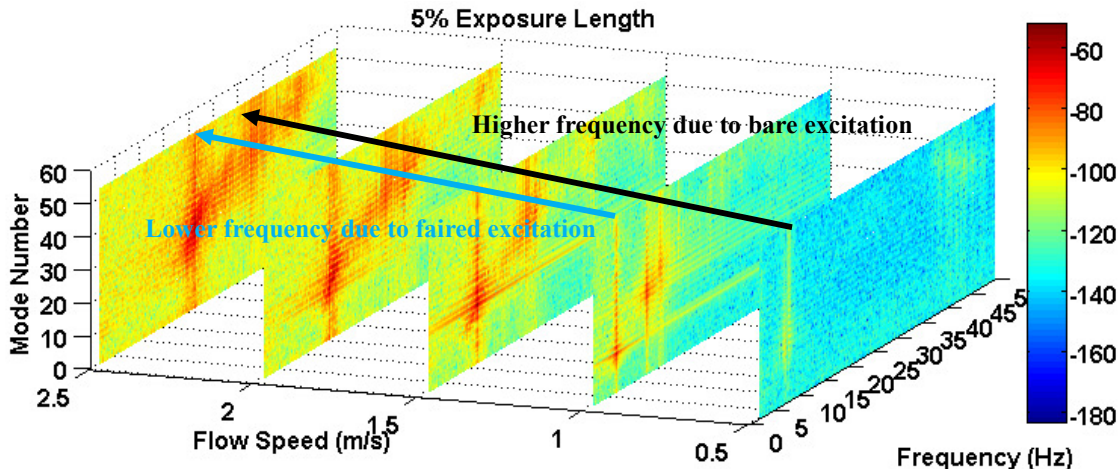
Figure 6: Volumetric slice plots for dispersion relation with 2D FFT to all curvatures for all test cases with 5% exposure length in the middle of pipe. In order to display all 2D FFT plots in one figure. A 5 second time window is used. The slices from lower flow speed to higher flow speed correspond to the Test2322, Test2321, Test2318, Test2319 and Test2320, respectively. The corresponding time sections are 66-71s ,48-53s, 33-38s, 28-33s and 24-29s. The black arrow from lower flow speed to higher flow speed represents the bare excitation at a higher frequency and the blue arrow from lower flow speed to higher flow speed represents the faired excitation at a lower frequency.

9

Copyright © 2012 by ASME
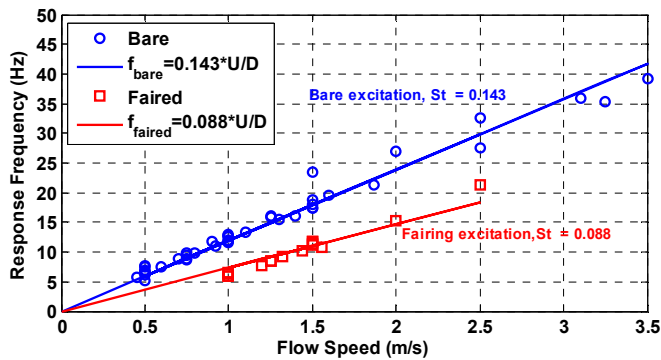
Figure 7: The frequency contents from fairing and bare were separated. Dominate peaks are plotted against flow speed for uniform flow. St for bare excitation is about 0.143 and for fairing excitation is about 0.088.
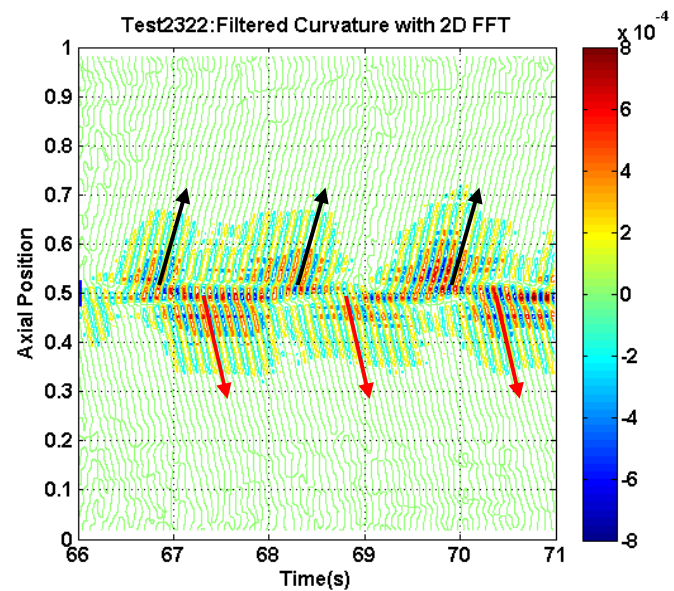

Figure 8 Contour plot of curvatures filtered by 2D FFT. The filtered parameters are 5-10Hz for wave frequency (f) and 10-45 for mode number corresponding to 0.83-3.72 for wave number (k).
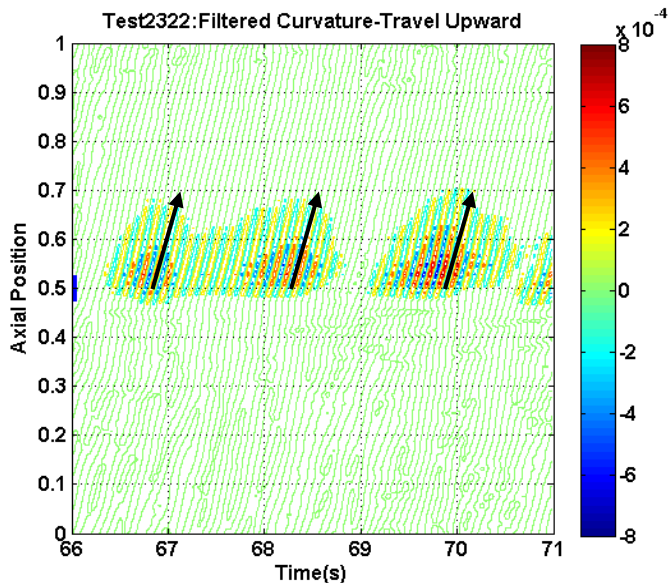

Figure 9: The traveling upward wave was separated from the total curvatures with 2D FFT. The 2D FFT was used to filter the original data. The filtering parameters are frequency from 5 to 10Hz and mode number from 10 to 45.
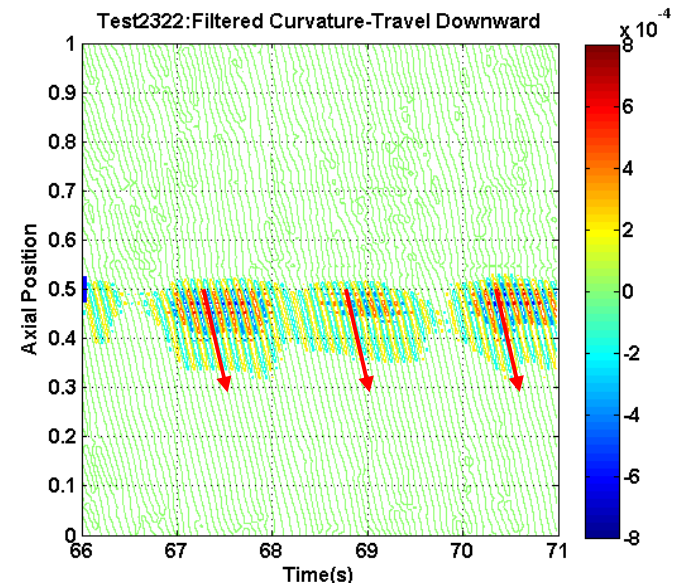
Figure 10: The traveling downward wave was separated from the total curvatures with 2D FFT. The 2D FFT was used to filter the original data. The filtering parameters are frequency from 5 to 10Hz and mode number from 10 to 45.

10

Copyright © 2012 by ASME

Test2322:25th Strain Gauge
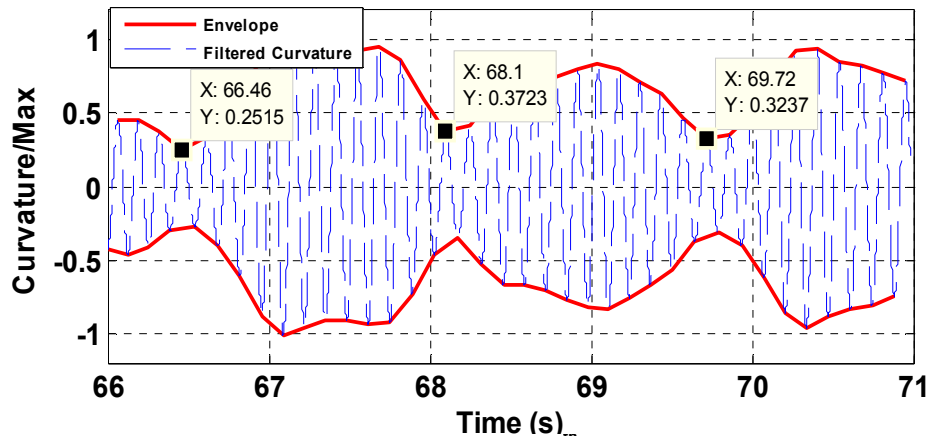
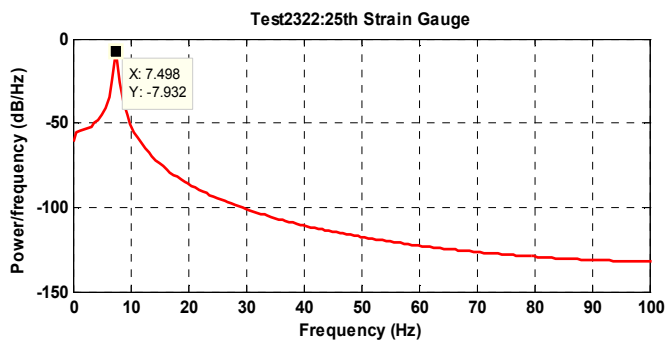Figure 11: Time history of the 25th strain gauge.

Figure 12 Spectrum of the 25th strain gauge with time window 66.5-68.1s. The 'pyulear' function in the MATLAB was used to get the spectrum plot. The peak frequency is 7.5Hz
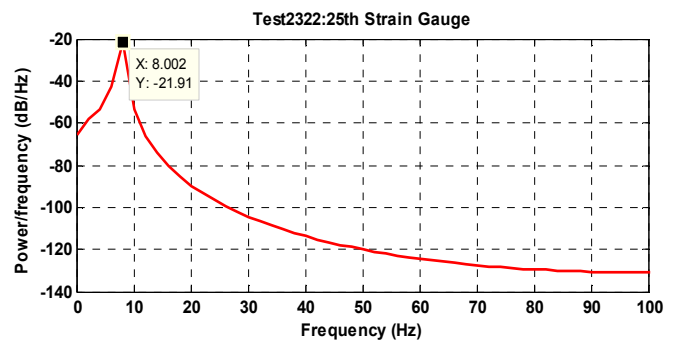

Figure 13 Spectrum of the 25th strain gauge with time window 68.1-69.7s. The 'pyulear' function in the MATLAB was used to get the spectrum plot. The peak frequency is 8.0Hz
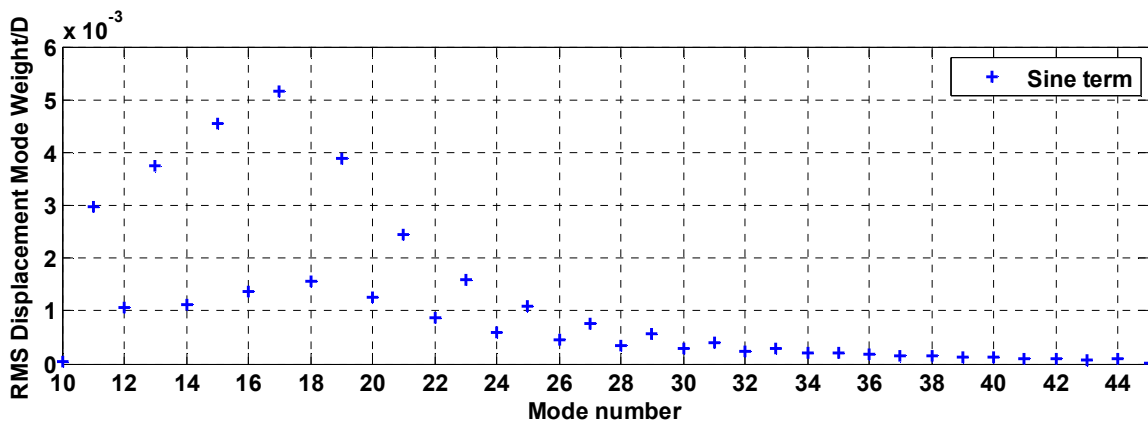

Figure 14: RMS displacement mode weights using sine terms from $n = 10$ to $n = 45$, almost 100 cycles corresponding to time window(66-90s) was used for reconstruction(Test 2322).

11   Copyright © 2012 by ASME
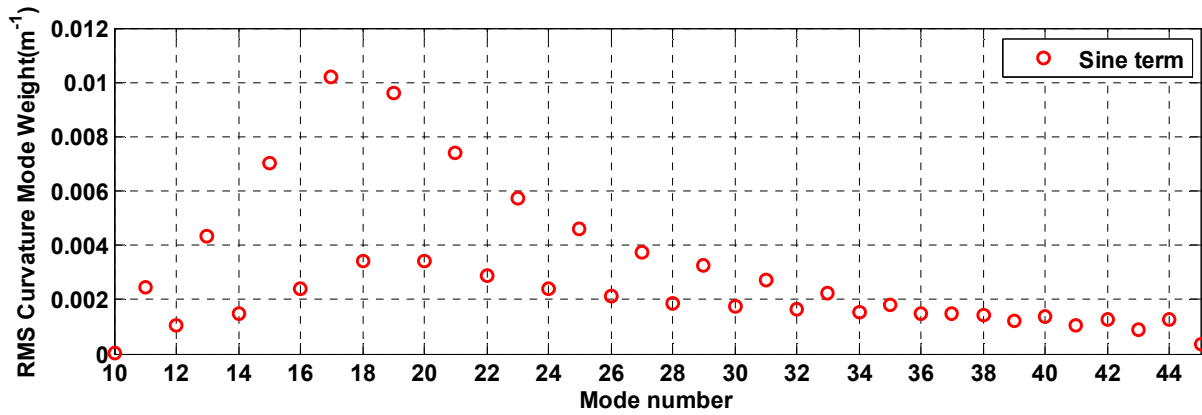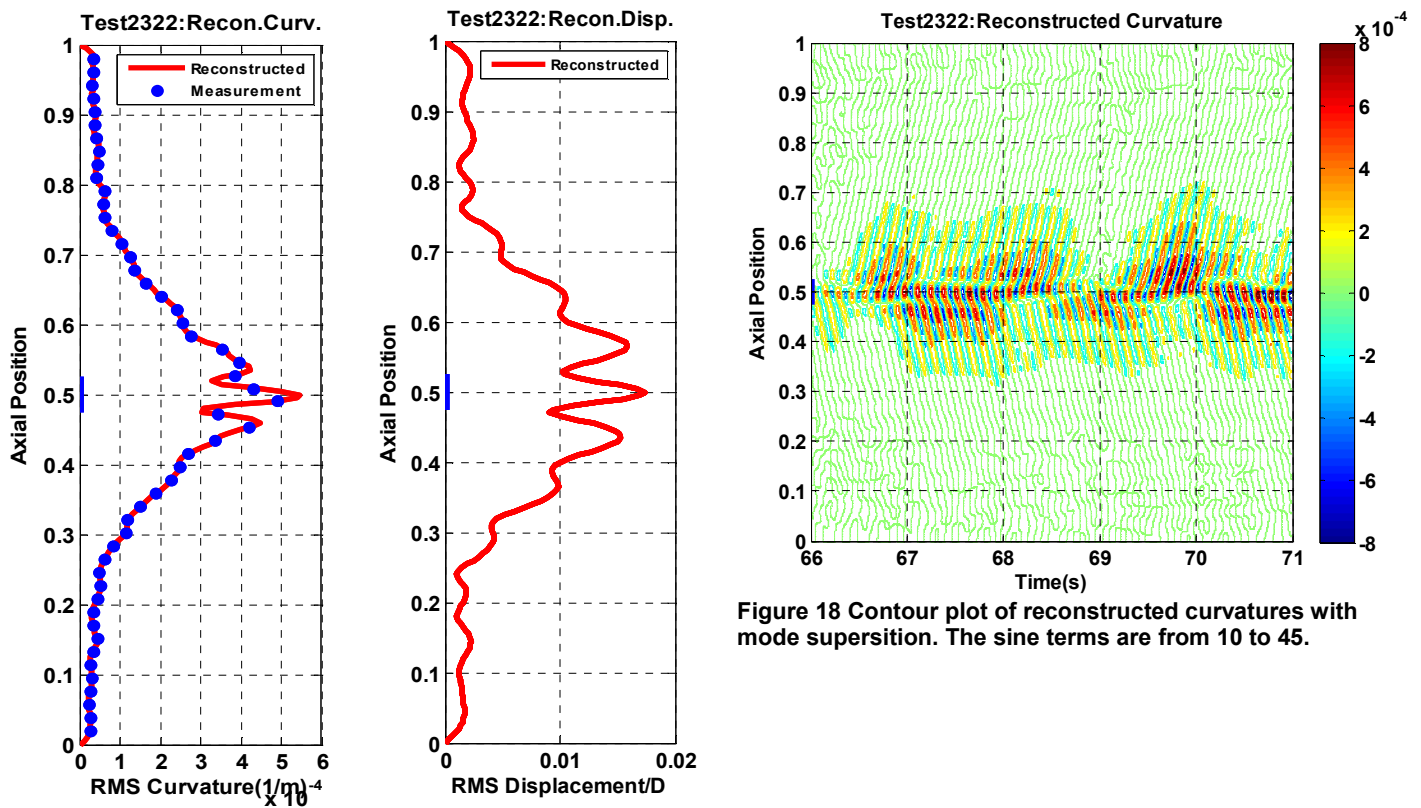
Figure 15: RMS curvature mode weights using sine terms from $n = 10$ to $n = 45$, almost 100 cycles corresponding to time window(66-90s) was used for reconstruction(Test 2322).

Figure 16: Reconstructed RMS curvatures (red line) for Test2322 using the sine terms from *n = 10* to *n = 45*, and 100 cycles (66-90s) was used for reconstruction.

Figure 17: Reconstructed RMS displacements (red line) for Test2322 using the sine terms from *n = 10* to *n = 45*, and 100 cycles (66-90s) was used for reconstruction.

Figure 18 Contour plot of reconstructed curvatures with mode supersition. The sine terms are from 10 to 45.
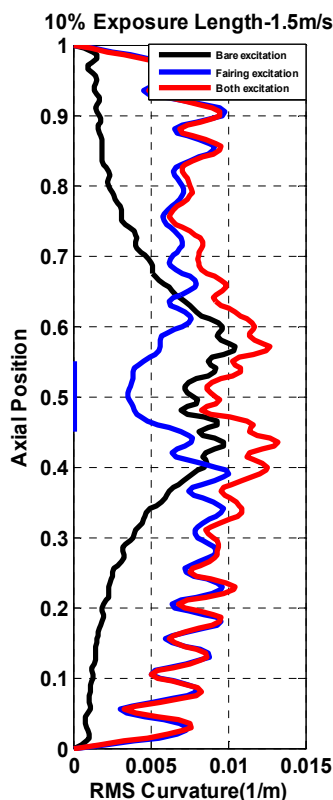
12   Copyright © 2012 by ASME

Figure 19: Reconstructed RMS curvatures for 10% exposure length under uniform flow speed U=1.5m/s. The blue, black and red lines represent RMS values of curvature due to faired, bare and total excitation, respectively(Test 2327).

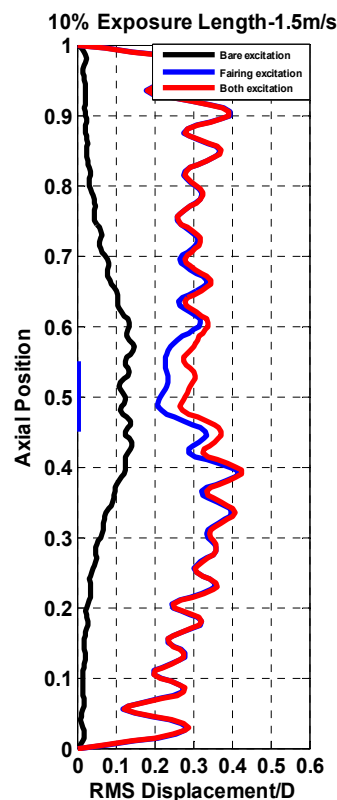**Figure 20: Reconstructed RMS displacements for 10% exposure length under uniform flow speed U=1.5m/s. The blue, black and red lines represent RMS values of curvature due to faired, bare and total excitation, respectively(Test 2327).**
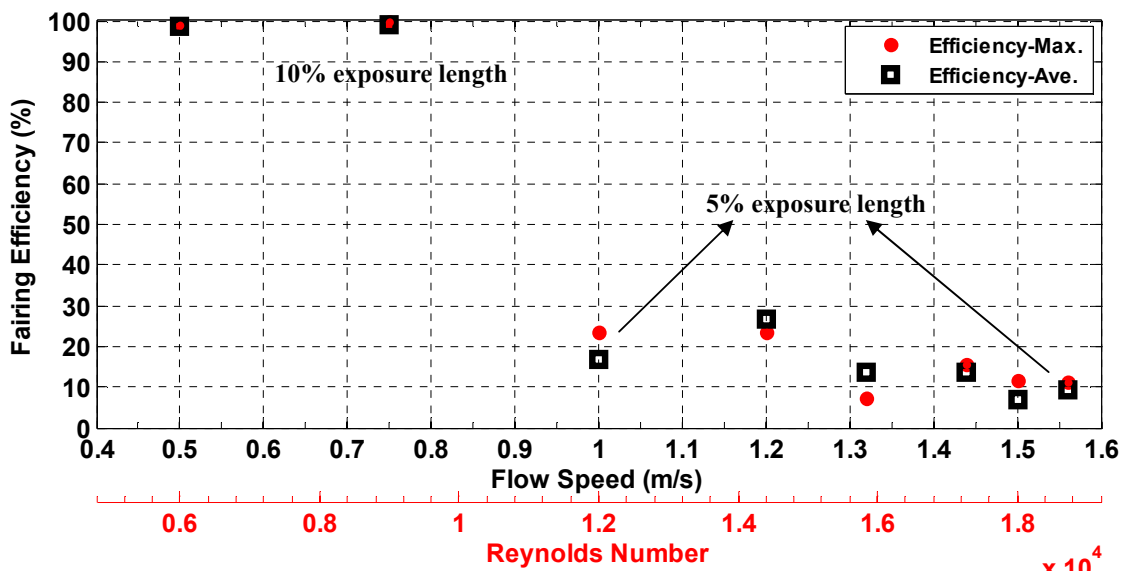

Fig.21: The efficiency of fairing in suppressing VIV. 100% means VIV is fully suppressed and 0% means VIV is never suppressed. The red dot stands for the efficiency of fairing estimated with the expression (16) and the black square stands for the efficiency of fairing estimated with the expression (15). The efficiencies of fairing at flow speed 0.75m/s, 1m/s and 1.5m/s were estimated with the expressions (17) and (18) for red dot and black square respectively.

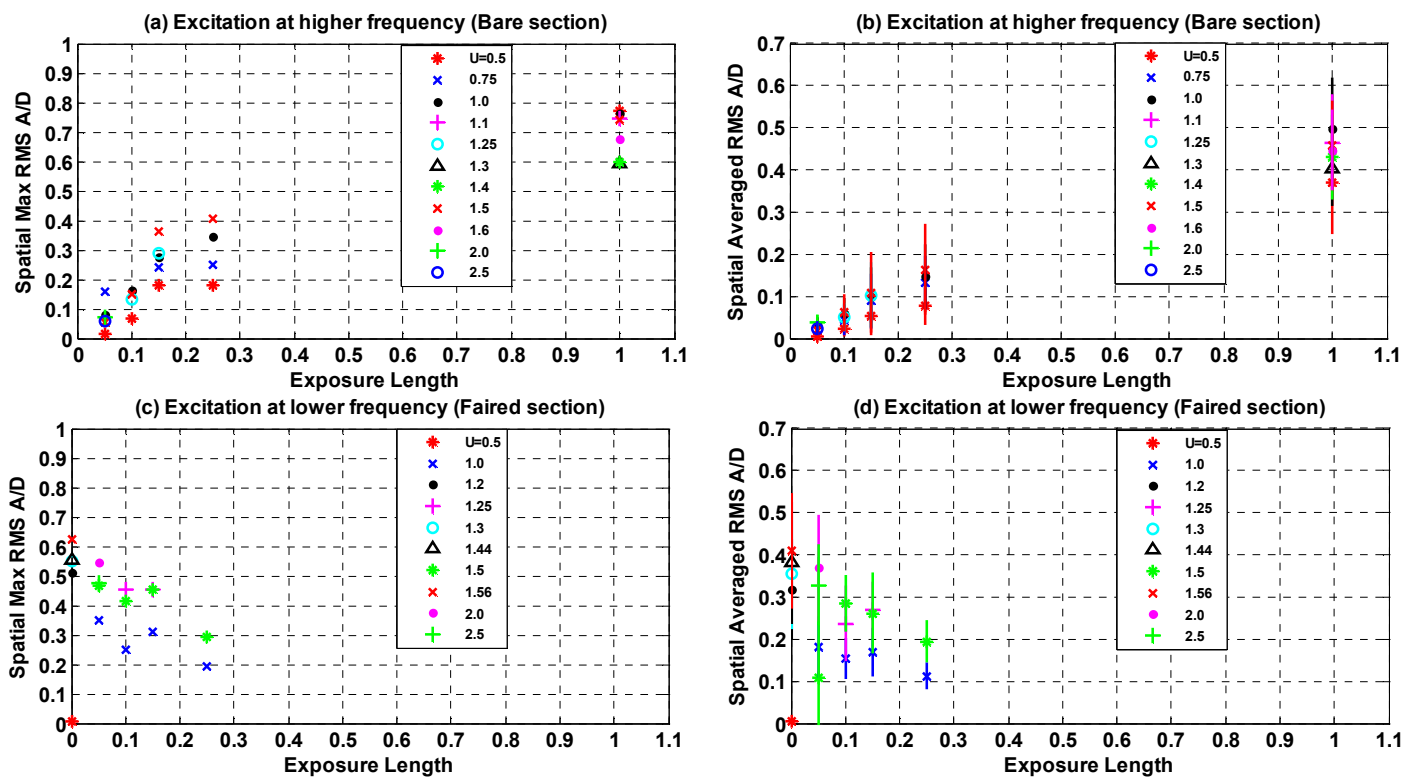13   Copyright © 2012 by ASME

Figure 22: The effect of exposure length on VIV. (a) The spatial maximum RMS A/D with exposure length due to bare excitation. (b) The spatial averaged RMS A/D with exposure length due to bare excitation. (c) The spatial maximum RMS A/D with exposure length due to fairing excitation. (d) The spatial averaged RMS A/D with exposure length due to fairing excitation. The bar represents the standard deviation of spatial RMS displacement.

14   Copyright © 2012 by ASME